Visual Inspection of DBS Efficacy

Brad E. Hollister*
California State University Dominguez Hills

Gordon Duffley†
University of Utah
Scientific Computing and Imaging Institute

Chris Butson‡
University of Utah
Scientific Computing and Imaging Institute

Chris Johnson§
University of Utah
Scientific Computing and Imaging Institute

Paul Rosen¶
University of South Florida

ABSTRACT

At present, approximately ten million people worldwide are afflicted by Parkinson's Disease (PD). One of the most promising therapies for PD is Deep Brain Stimulation (DBS). DBS works via stimulation of targeted central brain regions (nuclei), whose dysfunction is implicated in PD. A key problem with DBS is determining optimal parameters for clinical outcome. While multiple parameters may influence outcomes in DBS, we explore spatial correlation of volume of tissue activated (VTA) to Unified Parkinson's Disease Rating Scale (UPDRS) scores. Using the Neurostimulation Uncertainty Viewer (nuView), we investigate a number of cooperative visualizations for DBS inspection. Surface-to-surface Euclidean distance between VTA and selected brain nuclei are used in a linked 3D and parallel coordinates view of patient outcome. We then present a semivariogram-based approach to measure spatial correlation of patient outcomes with VTA. As a third component, nuView provides a unique visualization of an ensemble of electrode placements to reduce clutter and emphasize electrodes with spatially similar VTA. These methods corroborate a spatial aspect to DBS efficacy.

Index Terms: Human-centered computing—Visualization—Visualization design and evaluation methods

1 INTRODUCTION

Deep brain stimulation (DBS) is an established therapy for the treatment of Parkinson's disease (PD) and shows great promise for the treatment of several other disorders. However, while the clinical analysis of DBS has received great attention, a relative paucity of quantitative techniques exists to define the optimal surgical target and most effective stimulation protocol for a given disorder.

The Neurostimulation Uncertainty Viewer (nuView) [14] is currently used for visualizing the results of computational volume of tissue activated (VTA), with regard to patient outcome. In the context of DBS, VTA is defined as the volume of tissue stimulated at a threshold voltage, causing an axonal activation [5]. The main user group for nuView are bio-engineering researchers at the *Scientific Computing and Imaging Institute* (SCII). Continued development of nuView supports effective visualization of finite-element (FEM) simulation, and augments software such as SCIRun [15].

DBS research utilizes patient pre-operative Magnetic Resonance Imaging (MRI), electrode post-operative placement data, and post-operative brain anatomy via Computed Tomography (CT) or MRI. (CT scans are fused with pre-operative MRI.) See Fig. 1 for DBS research workflow.

VTA simulation is performed in a common coordinate space. Each patient's data is mapped to the common space using a non-linear diffeomorphic brain atlas [6]. Output from the patient-specific model pipeline results in a rectilinear grid of volumetric cells. For nuView ingestion, patient feedback data is stored volumetrically in activated cells corresponding to individual VTA.

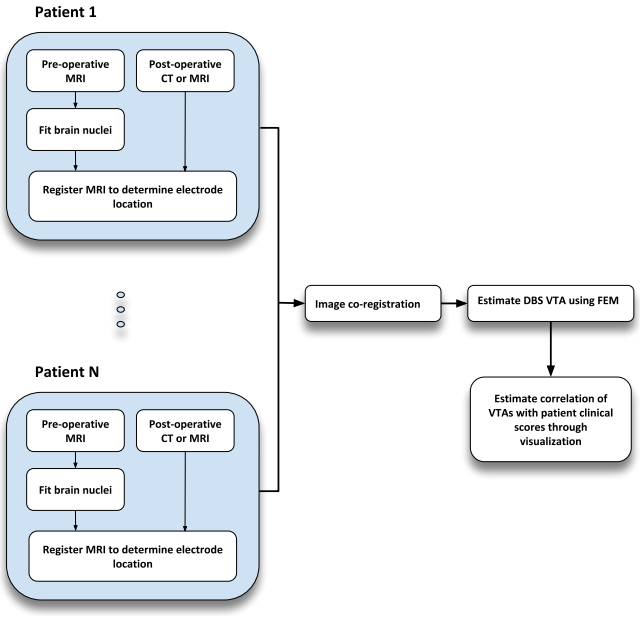

Figure 1: Patient ensemble and analysis of cohort. Sources of uncertainty: data acquisition, image registration algorithms, electrode geometry, lead location, DBS parameters, FEM for VTA, and clinical scores [6].

There is broad agreement that the effects of DBS for PD patients are critically dependent on stimulation location, and there has been growing recognition that analysis of previously implanted patients can be used to predict outcomes for future patients if three important factors are taken into account [6]. First, DBS parameters and electrode location(s) act synergistically in each patient and together they define the spread of stimulation to surrounding neural structures. Second, there is evidence to suggest that the optimal stimulation target of DBS may not be the subthalamic nucleus (STN) itself, but rather nearby structures. Third, there is substantial variability among PD patients with regard to the anatomical regions that are affected during DBS.

This paper's goal is the focused combination of newly applied methods to better understand, via interactive probing of the simulated VTA, quantitative aspects of the spatial correlation of VTA and patient outcome.

2 BACKGROUND

2.1 Visualization

The incorporation of uncertain data is now established visualization research [17, 27], and has been designated as a significant aspect of

*e-mail: bhollister@csudh.edu
†e-mail: gduffley@sci.utah.edu
‡e-mail: butson@sci.utah.edu
§e-mail: crj@sci.utah.edu
¶e-mail: prosen@usf.edu

IEEE VIS 2019
20-25 October, Vancouver, BC, Canada
978-1-7281-2016-4/19/$31.00 ©2019 IEEE

modern visual techniques [16]. Related to this work is inclusion of statistical metrics for isosurface extraction, linking multiple views of the data, and displaying explorations for parameter-space inspection and experimentation.

Isosurface extraction shows characteristics of three-dimensional scalar data. Probabilistic implementations of isocontours [30, 35] convey local uncertainty by distance from a mean [29]. These surfaces can represent shape and extent of clusters [24]. These earlier achievements relate to the current study, as patient outcome as a function of VTA is measured stochastically via ensemble simulation data.

Additional uncertainty visualization has been represented as transparency, glyphs, and color transfer [9, 18, 25, 33]. Fout and Ma [12] present an interactive tool to inspect uncertainty using a model that computes bounds on the uncertainty propagated by the volume rendering algorithm. Our work similarly uses volume rendering to visualize uncertainty. However, the represented uncertainty focuses on clinical outcome only.

An alternate way to consider statistical information is to include multiple values as PDFs, and use methods for classifying them. Research began by extending techniques to work with PDFs [26]. Slice planes [20] and clustering [4] can be used to reduce the data dimension for rendering, while colormaps, glyphs, and deformations have been used to express summaries and related groups of data [19, 21].

Three-dimensional representations are very useful for geometric structure representation and providing context. However, the complexity of data usually requires multiple presentation types to enable better understanding. Because of this, multi-window linked-view systems are popular for addressing uncertainty [11, 13, 31, 35]. DBS data in our research can be thought of in terms of parameter-space exploration. The effect of changes to input parameters can be linked to alternative views such as parallel coordinates [3].

Maries et al. [28], propose a visual comparison framework to explore correlation in neurological MRI volumes with patient mobility statistics, as a tool for early diagnosis and prevention. While their work focuses on mobility issues related to neurological data from an elderly cohort using similar interactively linked views, our paper presents the visualization challenges related to DBS lead location as a causative element in therapeutic outcome. A related work by Rosen et al. [34], proposed uncertainty visualization in a linked view for myocardial ischemia inverse simulation data. Parallel coordinates linked with a three-dimensional heart model allow users to interactively view probabilistic ensemble data. Our study, in addition to simulation data, focuses on uncertainty related to patient outcome versus simulation uncertainty.

2.2 Deep Brain Stimulation

A patient-specific computer model of DBS is a tool that can be used to implicate regions of the brain that are related to benefits and side effects of this surgical approach. A patient-specific model allows for visualization of the effects of DBS by using a reconstruction of an individual DBS lead (Fig. 2) on a neuro-anatomically correct morphed atlas and MRI scan, thereby allowing for direct quantification of lead location, neuro-anatomical regions of interest, and VTA (Fig. 3).

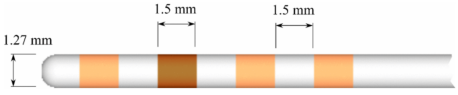

Figure 2: Medtronic DBS electrode Mo. 3387. Operational parameters for electrode are as follows; voltage: 1-5 V, frequency: 120-185 Hz, pulse width: 60-200 μs.

These models can be utilized to determine how much an individual effect is due to direct stimulation of a target region or due to overlap with other regions. When prescribing DBS there are two major variables that must be decided on an individual patient basis: 1) the electrode location, which is planned prior to surgery; 2) the stimulation protocol, which consists of the voltage, pulse width, frequency and configuration of anodes and cathodes. As our body of knowledge about DBS grows, we are identifying not only different stimulation targets for PD, such as the internal globus pallidus (GPi), but also sub-regions near each anatomical target that are correlated with specific motor or neuro-psychological outcomes.

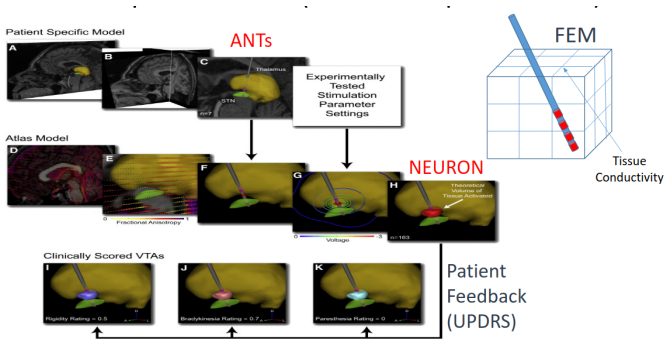

Figure 3: Patient-specific model pipeline, Butson et al. [6]. Anatomical Neurological Tomography (ANT) are shown as input, which is post-operative and fused with pre-operative MRI. FEM simulation is run by NEURON [7].

We have recently created a novel computational framework that integrates magnetic resonance imaging data, finite element electric field models, and predictions on the VTA generated by DBS on a patient-specific basis. The purposes of this framework are to: 1) predict the effects of DBS on an individual patient basis; 2) express VTAs from a multi-patient cohort in the context of an atlas brain; and 3) construct a patient specific atlas (PSA) that incorporates clinical outcomes. There is a summary of this approach from a recently-published prospective study [6]. Using this method we identified subregions around the STN where stimulation-induced activation was correlated with motor improvement on a per-symptom basis.

3 Methods

Multiple methods allow users to interactively experiment with patient subgroups and individual patient VTA. The various approaches are explained in the following sections. Each of the methods are shown both in a 3D interactive view and infographics panel view for a summarized comparison within or between loaded data sets. Each data set represents a different Unified Parkinson Disease Rating Scale (UPDRS) score and cohort.

Because of the complexity of the data, we have adopted a number of transfer functions to color the data, each designed to aid understanding in a unique way. A number of works provide guidelines for designing effective encodings [10, 36, 37]. However, colors and opacity are configurable (3D view, scatterplots, and glyphs), allowing individual users to select appropriate colors per use case.

3.1 Direct Volume Rendering

We provide a Direct Volume Rendering (DVR) of the UPDRS statistics of the VTA per voxel. The transfer functions use Piecewise Hermite functions to allow interpolation between points set by either the user or the tool itself. A DVR visualization is shown in Fig. 4. The initial treatment of the transfer functions and statistics were provided in [14], and explained here for clarity.

Value-based Coloring: Each statistic's range of values is mapped automatically by the tool, such that the minimum value is assigned to blue, the mean value to green, and the maximum value to red. For

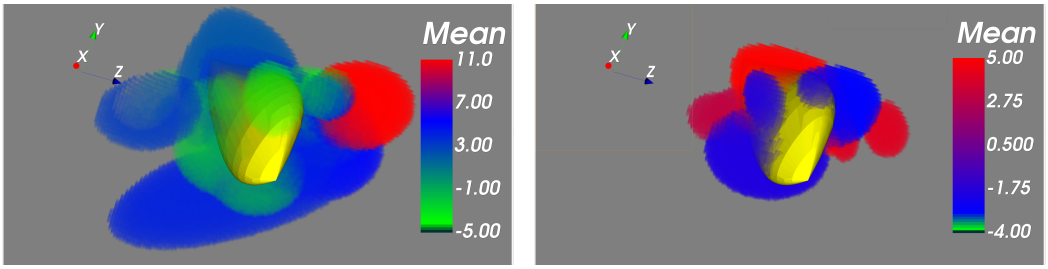

(a) (b)

Figure 4: (a) All patients in the data set cohort are shown with the mean UPDRS as a volume rendering. The transfer functions can be configured by the user. (b) Only a subset of the patients are included. The statistics update accordingly. The modeless subgroup dialog is shown in the upper right of the window.

transfer functions that are intended to allow the user to find given ranges of values in a particular statistic, opacity is initially set to fully opaque. The user can adjust any point in the transfer function.
Value-based Opacity: For the mean, maximum, minimum, and number of patients, we also provide opacity mapping via the tool. We normalize the opacities of each voxel based as a fraction of each voxel's own variance divided by the maximum variance from the data set. The variance is taken from the UPDRS scores. The lesser the variance in UPDRS score, the greater the applied opacity of the voxel is.

3.2 Semivariograms

Because the spatial coherence of VTA and clinical outcome is the subject of many studies in DBS therapy [6], we employ a common spatial statistic called the variogram to provide interactive probing of selected voxels at regular lag (distance to voxel) intervals. The semivariogram is discussed below.
Variogram Statistic: The empirical semivariance statistic is defined in Eq. 1,

$$\hat{\gamma}(h) = \frac{1}{2} \cdot \frac{1}{n(h)} \sum_{i=1}^{n(h)} (z(x_i + h) - z(x_i))^2 \qquad (1)$$

where z is a datum at a particular location, h is the distance between ordered data, and $n(h)$ is the number of paired data at a distance of h. The semivariance is half the variance of the increments $z(x_i + h) - z(x_i)$, but the whole variance of z-values at given separation distance h [1].

For a datum at lag distance h, we use UPDRS values along orthogonal directions from the location where we measure the semivariogram. While values can be changed to meet the needs of a particular data set, we increase h one voxel for each successive increment.

3.3 Surface-to-Surface Distance

The minimum Euclidean surface-to-surface distance is calculated between VTA and selected brain nuclei on a per vertex basis. Studies suggest high correlation between percent overlap (amount of VTA contained in target nuclei) and patient outcome [5]. We calculate the minimum distances via the algorithm presented in [2] (using the Visualization Toolkit's *vtkDistancePolyDataFilter* [32]), by first converting VTA voxels to a polygonal representation via marching cubes [23].

3.4 Electrode Ensemble

Our approach to an electrode ensemble view is based on *trajectory density projection* streamlines [22]. There, the trajectory density method is used to reduce clutter in streamline plots of high density. The 'Pick Up Sticks' visualization of Fig. 5 is a precursor to our method shown in Fig. 6.

We estimate electrode location based on principal component analysis of the VTA voxels. First we find the centroid, and then the principal component to find the direction of electrode placement. The electrode glyphs are defined by the point and direction.

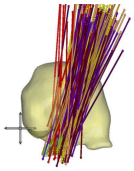

Figure 5: SCIRun's 'Pick Up Sticks' visualization of electrodes. This visualization is cluttered and does not easily show clusters or electrodes with similar VTA.

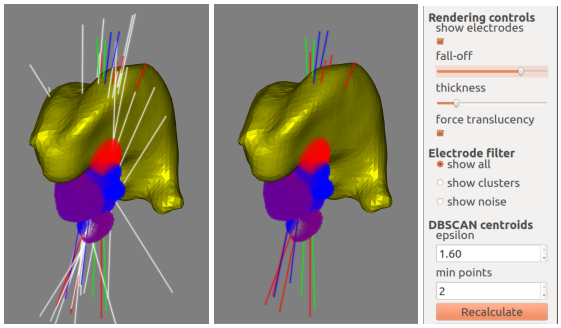

(a) (b) (c)

Figure 6: (a) Electrode glyphs are shown for Bradykinesia data set. Using DBSCAN, three clusters are shown in red, green, and blue. The white line (electrode) glyphs are noise. (b) The ensemble is considerably reduced in clutter by removing "noise" glyphs. Also shown is the control widget for glyph width and alpha blending falloff with DBSCAN parameter selection. (c) Modeless dialog allowing user to set electrode rendering and clustering parameters.

Rendering: We expand vertices in a polygon representing the electrode and blend alpha from the center. Each polygon is aligned with the camera, as to be facing it when camera rotations are introduced.
Clustering: Users may specify parameters for density-based spatial clustering of applications with noise (DBSCAN), to determine electrode clusters with associated VTA centroids. Clustering is independent of the principal component of the VTA. After clustering, the user can select to view noise or the clusters only, greatly simplifying

the visualization. Additionally, users can specify subgroups of the patient cohort, further reducing clutter by showing only selected clusters.

4 Results

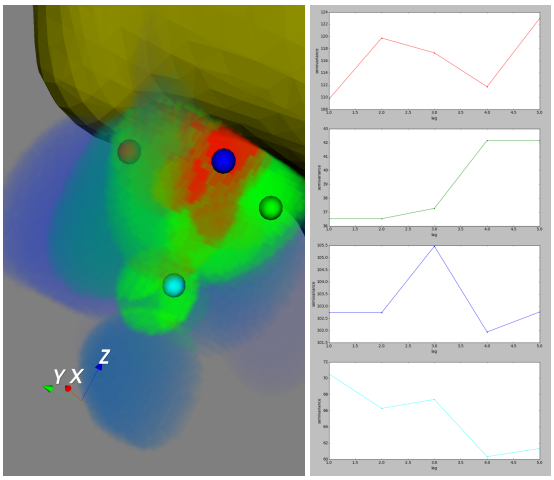

Figure 7: Semivariance is shown for each of the selected regions of the VTA. Each region is specified by a colored spherical glyph and the semivariance plot on the right has the corresponding color. Note that the DVR has a separate color mapping not shown.

Using our tool, we first discuss the semivariogram plots in relation to spatial correlation of VTA outcomes. Secondly, we discuss how our electrode view and outcomes vary across clusters of VTA centroids. Finally, we show distance variation and outcomes are weakly correlated on this metric alone, as interpreted by our data sets and visualization.

The data input into our system consists of a four-dimensional array. The fourth dimension is the patient outcome, which varies from seventeen to twenty-four from different data sets (UPDRS scores). The first three dimensions are the spatial extents for the simulation, here 120 x 120 x 120 voxels.

Semivariogram: Figure 7 displays various locations (color coded) and their linked view with the semivariogram at voxel values taken at distances represented in units of voxels from the selected location(s). For this representative figure, only the cyan location shows a semivariogram with a marked decreasing amount of semivariance at samples taken progressively more distant from the central voxel. While that position is comparable in variance with the other selected voxels (histogram not shown), it is also at the periphery of the simulated VTA. It is likely to be an artifact of data sparsity and that the majority of the samples taken are from disproportionately fewer participating VTA. Otherwise, most semivariograms suggest spatial correlation, although not necessarily spherical covariance [8].

Electrode clusters: Figure 6 improves upon Fig. 5, where both VTA uncertainty (clusters) and clutter (blended transparency of glyphs) help users to identify similar VTA based on location. Using a parallel coordinates view of patients belonging to clusters, the outcomes of those patients can be compared. Figure 8, shows disparities in patient outcome. Because clustering is based on VTA centroids, this suggests that the location of the VTA is also important in determining the UPDRS scores.

Brain nucleus distance: Figure 9 shows VTA surface-to-surface distance to a GPi. On the right, in the parallel coordinates view, the minimum distance of each VTA is graphed for comparison with patient outcomes (lower parallel coordinates view). Again, there are some signs of correlation with overall minimum distance between the surfaces of target brain nuclei and VTA, but this inquiry suggests

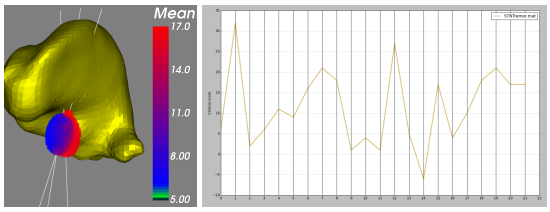

Figure 8: On the left, we show a cluster of VTA based on centroid location. The patient mean scores are not the same, but exhibit similar improvement in UPDRS. The patient numbers for the cluster members are 3, 6, and 15. Their UPDRS scores can be seen in the parallel coordinates view as approximately 5, 10, and 17, respectively.

the need for a more comprehensive and subtle map of neural circuitry to provide stronger correlation. This form of visualization does provide insight into whether given targets are effective or not given locality, however.

A concern of domain experts, is the need for patient meta-data. As there may be other issues related to efficacy other than electrode placement and parameters, correlation with variables such as medications, age, and length of treatment are all necessary components for proper therapeutic assessment. Another observation, is the need of larger cohorts for statistical significance. This is not a direct issue with the software, as the only available cohorts at the time of research were twenty-four or less. Larger patient populations, however, are anticipated to require some interface redesign. Such design issues could affect infographic layout and dialog selections of patient inclusion, or exclusion, in analysis.

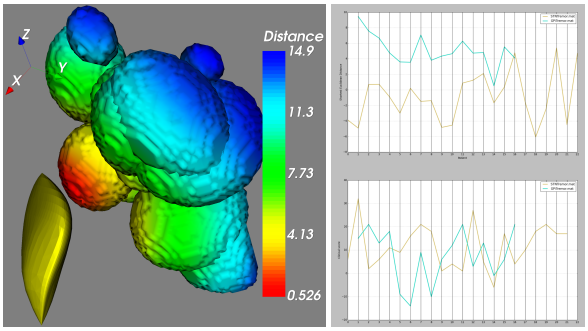

Figure 9: 3D view displays surface-to-surface Euclidean distance for VTA and GPi for the 'STN Tremor' data set. The topmost parallel coordinates shows shortest distance per patient VTA, whereas the bottom graph contains patient scores.

5 Conclusion and Future Work

As our examples show, nuView supports earlier research that suggest lead location is a strong predictor of patient outcome. However, the tool also identifies exceptions to this assumption. We plan to extend nuView to support patient meta-data (such as age, drugs, etc.). This extension will allow researchers to investigate the degree of possible influence on clinical outcomes as a result of other factors used in tandem with lead location. It is also anticipated that such additional information will benefit clinicians in the treatment of individual patients, as their personal profile may weigh heavily on optimal therapy.

Acknowledgments

This project was supported in part by the National Institute of General Medical Sciences of the NIH under grant number P41 GM103545-17, and by National Science Foundation grants IIS-1845204.

REFERENCES

[1] M. Bachmaier and M. Backes. Variogram or semivariogram? understanding the variances in a variogram. *Precision Agriculture*, 9(3):173–175, 2008.

[2] J. A. Baerentzen and H. Aanaes. Signed distance computation using the angle weighted pseudonormal. *Visualization and Computer Graphics, IEEE Transactions on*, 11(3):243–253, 2005.

[3] W. Berger, H. Piringer, P. Filzmoser, and E. Gröller. Uncertainty-aware exploration of continuous parameter spaces using multivariate prediction. In *Computer Graphics Forum*, vol. 30, pp. 911–920. Wiley Online Library, 2011.

[4] U. D. Bordoloi, D. L. Kao, and H.-W. Shen. Visualization techniques for spatial probability density function data. *Data Science Journal*, 3:153–162, 2004.

[5] C. Butson, S. Cooper, J. Henderson, and C. McIntyre. Patient-specific analysis of the volume of tissue activated during deep brain stimulation. *NeuroImage*, 34(2):661–670, January 2007. doi: 10.1016/j.neuroimage.2006.09.034

[6] C. R. Butson, S. E. Cooper, J. M. Henderson, B. Wolgamuth, and C. C. McIntyre. Probabilistic analysis of activation volumes generated during deep brain stimulation. *Neuroimage*, 54(3):2096–2104, 2011.

[7] N. T. Carnevale and M. L. Hines. *The NEURON book*. Cambridge University Press, 2006.

[8] J.-P. Chiles and P. Delfiner. *Geostatistics: modeling spatial uncertainty*, vol. 497. John Wiley & Sons, 2009.

[9] S. Djurcilov, K. Kim, P. Lermusiaux, and A. Pang. Visualizing scalar volumetric data with uncertainty. *Computers & Graphics*, 26(2):239–248, 2002.

[10] J. Eckstut and A. Eckstut. *The secret language of color: Science, nature, history, culture, beauty of red, orange, yellow, green, blue & violet*. Black Dog & Leventhal Publishers, 2013.

[11] D. Feng, L. Kwock, Y. Lee, and R. M. Taylor II. Linked exploratory visualizations for uncertain mr spectroscopy data. In *IS&T/SPIE Electronic Imaging*, pp. 753004–753004. International Society for Optics and Photonics, 2010.

[12] N. Fout and K.-L. Ma. Fuzzy volume rendering. *Visualization and Computer Graphics, IEEE Transactions on*, 18(12):2335–2344, 2012.

[13] S. Haroz, K.-L. Ma, and K. Heitmann. Multiple uncertainties in time-variant cosmological particle data. In *Visualization Symposium, 2008. PacificVIS'08. IEEE Pacific*, pp. 207–214. IEEE, 2008.

[14] B. Hollister, G. Duffley, C. Butson, C. Johnson, and P. Rosen. Visualization for understanding uncertainty in activation volumes for deep brain stimulation. *EuroVis-Short Papers*, 2016.

[15] S. Institute, 2015. SCIRun: A Scientific Computing Problem Solving Environment, Scientific Computing and Imaging Institute (SCI), Download from: http://www.scirun.org.

[16] C. Johnson. Top scientific visualization research problems. *Computer graphics and applications, IEEE*, 24(4):13–17, 2004.

[17] C. R. Johnson and A. R. Sanderson. A next step: Visualizing errors and uncertainty. *Computer Graphics and Applications, IEEE*, 23(5):6–10, 2003.

[18] A. J. Joseph, S. Lodha, J. Renteria, and A. Pang. Uisurf: Visualizing uncertainty in isosurfaces. Master's thesis, University of California, Santa Cruz, 1998.

[19] D. Kao, J. L. Dungan, and A. Pang. Visualizing 2d probability distributions from eos satellite image-derived data sets: A case study. In *Visualization, 2001. VIS'01. Proceedings*, pp. 457–589. IEEE, 2001.

[20] D. Kao, A. Luo, J. L. Dungan, and A. Pang. Visualizing spatially varying distribution data. In *Information Visualisation, 2002. Proceedings. Sixth International Conference on*, pp. 219–225. IEEE, 2002.

[21] J. M. Kniss, R. Van Uitert, A. Stephens, G.-S. Li, T. Tasdizen, and C. Hansen. Statistically quantitative volume visualization. In *Visualization, 2005. VIS 05. IEEE*, pp. 287–294. IEEE, 2005.

[22] A. Kuhn, N. Lindow, T. Günther, A. Wiebel, H. Theisel, and H.-C. Hege. Trajectory density projection for vector field visualization. *EuroVis-Short Papers*, pp. 31–35, 2013.

[23] W. E. Lorensen and H. E. Cline. Marching cubes: A high resolution 3d surface construction algorithm. In *ACM siggraph computer graphics*, vol. 21, pp. 163–169. ACM, 1987.

[24] A. Lucieer. Visualization for exploration of uncertainty related to fuzzy classification. In *Geoscience and Remote Sensing Symposium, 2006. IGARSS 2006. IEEE International Conference on*, pp. 903–906. IEEE, 2006.

[25] C. Lundstrom, P. Ljung, A. Persson, and A. Ynnerman. Uncertainty visualization in medical volume rendering using probabilistic animation. *Visualization and Computer Graphics, IEEE Transactions on*, 13(6):1648–1655, 2007.

[26] A. Luo, D. Kao, and A. Pang. Visualizing spatial distribution data sets. In *VisSym*, 2003.

[27] A. M. MacEachren, A. Robinson, S. Hopper, S. Gardner, R. Murray, M. Gahegan, and E. Hetzler. Visualizing geospatial information uncertainty: What we know and what we need to know. *Cartography and Geographic Information Science*, 32(3):139–160, 2005.

[28] A. Maries, N. Mays, M. Hunt, K. F. Wong, W. Layton, R. Boudreau, C. Rosano, and G. E. Marai. Grace: A visual comparison framework for integrated spatial and non-spatial geriatric data. *IEEE transactions on visualization and computer graphics*, 19(12):2916–2925, 2013.

[29] K. Pöthkow and H.-C. Hege. Positional uncertainty of isocontours: Condition analysis and probabilistic measures. *Visualization and Computer Graphics, IEEE Transactions on*, 17(10):1393–1406, 2011.

[30] K. Pöthkow, B. Weber, and H.-C. Hege. Probabilistic marching cubes. In *Computer Graphics Forum*, vol. 30, pp. 931–940. Wiley Online Library, 2011.

[31] K. Potter, A. Wilson, P.-T. Bremer, D. Williams, C. Doutriaux, V. Pascucci, and C. R. Johnson. Ensemble-vis: A framework for the statistical visualization of ensemble data. In *Data Mining Workshops, 2009. ICDMW'09. IEEE International Conference on*, pp. 233–240. IEEE, 2009.

[32] C. Quammen, C. Weigle, and R. Taylor. Boolean operations on surfaces in vtk without external libraries. *Insight J*, 797:1–12, 2011.

[33] P. J. Rhodes, R. S. Laramee, R. D. Bergeron, T. M. Sparr, et al. Uncertainty visualization methods in isosurface rendering. In *Eurographics*, vol. 2003, pp. 83–88, 2003.

[34] P. Rosen, B. Burton, K. Potter, and C. Johnson. Visualization for understanding uncertainty in the simulation of myocardial ischemia. In *Proceedings of the 2013 Workshop on Visualization in Medicine and Life Sciences*, 2013.

[35] J. Sanyal, S. Zhang, J. Dyer, A. Mercer, P. Amburn, and R. J. Moorhead. Noodles: A tool for visualization of numerical weather model ensemble uncertainty. *Visualization and Computer Graphics, IEEE Transactions on*, 16(6):1421–1430, 2010.

[36] M. Stone. *A field guide to digital color*. AK Peters/CRC Press, 2016.

[37] C. Ware. *Information visualization: perception for design*. Elsevier, 2012.